Site-selective spectroscopy of Er^{3+}:Ti:LiNbO$_3$ waveguides

V. Dierolf[1,*], **A.B. Kutsenko**[1,**], **A. Ostendorf**[1], **W. von der Osten**[1], **W. Sohler**[2], **H. Suche**[2]

[1] Experimentalphysik, Fachbereich 6, Universität-GH Paderborn, 33095 Paderborn, Germany
[2] Angewandte Physik Fachbereich 6, Universität-GH Paderborn, 33095 Paderborn, Germany

Abstract. Starting from previous investigations in LiNbO$_3$ bulk crystals, we studied the optical properties of Er^{3+} ions in Ti:LiNbO$_3$ channel waveguides and investigated the waveguide-specific lattice environment of the Er^{3+} ions ("sites") caused by the doping method used and the presence of a large number of Ti^{4+} ions. For that purpose the method of combined excitation–emission spectroscopy was applied for the first time to waveguides at low temperatures. Comparing the spectroscopic results obtained for the green, red, and near-IR luminescence ($\lambda \approx 550$, ≈ 650 and ≈ 980 nm) under direct (450 nm), 2-step (980 nm), and 3-step (1.5 μm) laser excitation, we found several distinguishable Er^{3+} sites which in terms of energy levels and relative numbers are similar to those in bulk material, but exhibit significantly different upconversion efficiencies and strongly inhomogeneously broadened transitions. Moreover, we were able to distinguish isolated and cluster Er^{3+} sites by their characteristic excitation and emission transition energies and studied the respective excitation/relaxation channels. The cluster sites are most efficient in the up-conversion process, especially under 3-step excitation. Using accepted microscopic models for Er^{3+} and Ti^{4+} incorporation into the LiNbO$_3$ crystal lattice, the site distribution and up-conversion mechanisms are elucidated and their consequences for laser applications in different spectral regions are discussed.

PACS: 42.82.Et; 71.70.Ch; 77.84.Dy

Lithium niobate (LiNbO$_3$) is one of the most attractive materials in the field of integrated optics. Besides its well-known intrinsic properties, LiNbO$_3$ offers the possibility to produce low-loss waveguides and to incorporate laser active ions (e.g., Er^{3+}) via diffusion doping [1–3]. Based on this already quite advanced technology, numerous active integrated optical components have been realized. For example, a whole family of Er^{3+} lasers in the important 1.5 μm spectral region has been demonstrated [2], including cw lasers as well as Q-switched, acousto-optically tunable, mode-locked and narrow-band DBR(distributed Bragg reflector)-type lasers. Besides this well-studied 1.5 μm transition from the first excited to the ground state, in principle the Er^{3+} ion offers more possibilities for laser operation, as shown in Fig. 1. For instance lasing in the MIR (3 μm) and visible (550 nm) has been demonstrated under NIR pumping at 980 nm for other host materials (e.g., YAG, LiYF$_4$, and glass fibers; see, e.g., [4]). The excitation of the respective emission transitions involves more complicated pump and relaxation schemes, including up-conversion and cross-relaxation. While being essential to the realization of 550 nm and 3 μm lasers, these
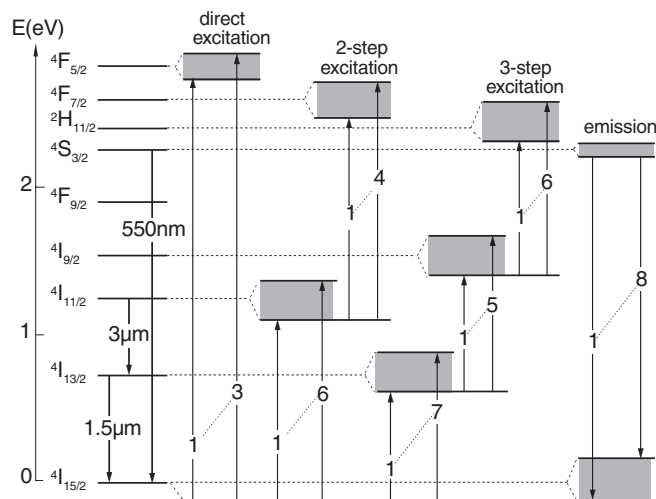

Fig. 1. Energy level diagram of Er^{3+} in LiNbO$_3$ and the main transitions relevant to this paper. Stark splittings for some states are schematically shown by the *shaded area*. The transitions from the lowest sublevel of the initial states are labeled by numbers according to the multiplicity of the final states

*Corresponding author. (Fax: +1-610/758-5730, E-mail: vod2@lehigh.edu)
Present address: Dept. of Physics, Lehigh University, 16 Memorial Drive East, Bethlehem, PA 18015, USA
**Permanent address:* A.F. Ioffe Phys.-Techn. Inst., 194021 St. Petersburg, Russia

processes are all detrimental to the performance of devices operating at 1.5 μm. In any case a sound understanding of the excitation processes at various pump wavelengths is necessary.

In the case of Er^{3+}-doped $LiNbO_3$, spectroscopic studies have been limited essentially to bulk material. Due to these results [5–9], it is commonly accepted that the Er^{3+} ions are located in slightly different lattice environments ("sites") which depend on the method of crystal preparation. Therefore we expected – and actually observed in a preliminary study [10] – that the production of waveguide structures by diffusion of Ti^{4+} ions into the surface of an $LiNbO_3$ wafer creates within the wave-guiding zone specific conditions for Er^{3+} ions and their crystalline environment. Moreover, it turned out that the up-conversion efficiencies are very sensitive to the energetic position of the respective transitions, making any extrapolation of the results from bulk material to waveguides questionable.

While only a few preliminary results [10, 11] exist, a comprehensive study of the Er^{3+} defect in $LiNbO_3$ waveguides at low temperatures is missing so far. With this paper we fill this gap addressing especially the following questions:

1. How do the methods of Er^{3+} doping (i.e., by diffusion or in the melt) and the presence of Ti^{4+} ions influence the types and relative number distribution of Er^{3+} sites?
2. How is the disorder induced by the high Ti^{4+} concentration reflected in the optical properties of the Er^{3+} ions within the waveguide?
3. Which kind of up-conversion processes occur under IR-pumping and to what extent do the different Er^{3+} sites participate?

After a brief description of the sample preparation (Sect. 1), the spectroscopic method will be described and examples for the data sets obtained will be presented in Sect. 2. The complete set of measurements is further evaluated and discussed in Sect. 3, focussing on answers to the questions above. Finally in Sect. 4 the results will be summarized.

1 Sample preparation

The channel waveguides were fabricated on commercially available (congruent) $LiNbO_3$ z-cut wafers using the well-established technique of Er and Ti in diffusion.

For laser applications and for our study, which both require Er^{3+} doping near the surface, an Er metal layer (11 nm thickness) is brought onto the substrate as a first step and is diffused at $T_d \approx 1130\,°C$ (just below the Curie temperature) into the $LiNbO_3$ wafer for a duration of $t_d = 100\,h$. The diffusion doping proves to be a rather simple and most efficient technique which yields doping levels in the surface regions close to the solubility limit without sacrificing the optical quality of the wafer. On the basis of earlier experimental and theoretical studies of this diffusion process [12, 13] the resulting Er^{3+} doping profile can be calculated and is shown in Fig. 2. These modelling results are consistent with the absorption spectrum around 1.5 μm that we obtained for our samples.

In a second step photolithographically defined Ti stripes are diffused into the wafer using again previously determined optimized parameters for the layer thickness (100 nm) and
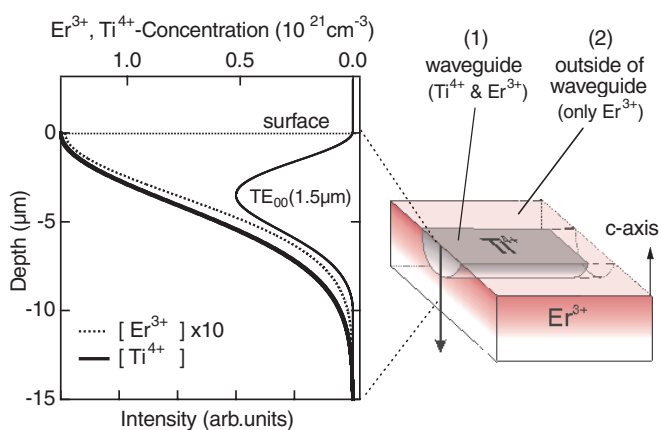

Fig. 2. Calculated Ti^{4+} and Er^{3+} doping profiles and TE_{00} mode intensity distributions in a 1.5 μm single-mode $Ti:LiNbO_3$ channel waveguide. On the right, a waveguide sample is depicted schematically and two spatial regions [(1) and (2)] for which measurements were performed are indicated

stripe width (7 μm) as well as for the diffusion time (9 h) and temperature (1060 °C). In that way, we obtained single-mode waveguides for 1.5 μm with losses as low as 0.2 dB/cm. The calculated Ti diffusion profile and the spatial intensity distribution of the propagating 1.5 μm pump wave are shown in Fig. 2 for the TE_{00} mode. The small cross-section already yields excitation densities of $2\,kW/cm^2$ at moderate pump power (1 mW).

2 Experimental method and results

Earlier studies on $LiNbO_3$ bulk material have shown that the method of combined excitation–emission spectroscopy (CEES) is a powerful tool for site-selective investigations [6, 9, 14]. In this technique we take advantage of an optical multichannel analyzer (SI IRY700) which allows a large number of emission spectra to be recorded for a dense sequence of excitation energies within a fairly short time without moving the spectrometer grating. In that way a very good spectral reproducibility and, hence, good site selectivity can be achieved. The resulting two-dimensional data set of emission intensities as a function of emission and excitation photon energies is best visualized using a contour plot in which lines of equal emission intensities are drawn. In this representation of the data the spectral responses of Er^{3+} ions which are situated in different crystal environments and have altered transition energies can easily be distinguished.

The main experimental challenge in applying CEES to waveguide samples at low temperatures is the necessity to ensure an efficient and stable coupling of the light into the waveguide. For that purpose we constructed a special setup: As the central component we used an He-gas flow cold finger cryostat (Oxford Microstat^{He}) with a high numerical aperture. The cryostat was mounted on kinematic translational and rotational stages allowing the adjustment of position and angle with high precision (1 μm, 1″). That accurate adjustability also helped to probe and distinguish emission originating from spots within and outside the wave-guiding zones (see Fig. 2). In order to avoid a high level of stray light, we employed single-mode fibers acting as spatial filters for the excitation light. The light exiting the fiber was coupled

into the waveguide with two microscope lenses, using the easily visible green emission for optimization. The required long integration times (1 min) and the inevitable mechanical instability made mode-selective excitation impossible, especially for wavelengths higher than 1.5 µm, and therefore only time- and mode-averaged results were obtained. The portion of the emission light which was guided through our sample was further spatially filtered using a small pinhole before it entered a conventional grating monochromator. The spectral resolution of the monochromator was always better than 0.25 meV, sufficient to resolve all spectral features. In tuning the exciting lasers, we chose a step size of the same order (0.1 meV), although the laser linewidths were much less (10 GHz to 100 kHz).

In the majority of our experiments we detected the emission in the green ($^4S_{3/2} \rightarrow {}^4I_{15/2}$) spectral region, for which three distinctively different excitation/relaxation schemes (indicated in Fig. 1) could be investigated:

- A direct ("1-step") excitation scheme ($^4I_{15/2} \rightarrow {}^4F_{5/2}$) using a tunable dye laser (≈ 450 nm, 20 mW) pumped by the UV lines of an Ar^+ laser.
- An up-conversion ("2-step") excitation scheme ($^4I_{15/2} \rightarrow {}^4I_{11/2} \rightarrow {}^4F_{7/2}$) using a tunable Ti:sapphire laser (≈ 980 nm, 60 mW).
- An up-conversion ("3-step") excitation scheme ($^4I_{15/2} \rightarrow {}^4I_{13/2} \rightarrow {}^4I_{9/2} \rightarrow {}^2H_{11/2}$) using a tunable external cavity semiconductor laser (≈ 1.5 µm, 6 mW).

The specified laser powers were measured at the output of the respective single-mode fiber. The power coupled into the waveguide was still considerably less due to the multiple surfaces and the detrimental influence of the cryostat window on the mode profile. For the resulting in-coupled laser power levels, no significant optical damage could be observed and the spectral line shapes were power independent.

The contour plots of the corresponding CEES measurements are depicted in the comprehensive Fig. 3. While for the 1- and 2-step cases the complete spectral range of excitation is depicted, due to the limited tunability of the external cavity laser, the 3-step excitation at 1.5 µm is restricted to only five of a possible seven $^4I_{15/2} \rightarrow {}^4I_{13/2}$ transitions. In all cases five (out of eight) emission transitions from the lowest $^4S_{3/2}$ sublevel to the five lowest Stark levels of the $^4I_{15/2}$ ground state are shown. The small shaded boxes in Fig. 3 mark the spectral range of these transitions for the regular sites, which will be discussed below.

In a similar way different emission transitions in the red ($^4F_{9/2} \rightarrow {}^4I_{15/2}$ and $^4I_{11/2} \rightarrow {}^4I_{15/2}$) as well as different polarization conditions have been studied for our waveguide samples.[1] For a reliable comparison also bulk material was measured under the same experimental conditions. All measurements were performed at a sample temperature of ≈ 10 K.

3 Data evaluation and interpretation

The complete set of measured CEES data represents a solid basis to investigate the questions raised above. For that purpose the data need to be further evaluated, and selected excerpts of them will be shown in different ways such that the various aspects are elucidated most clearly.

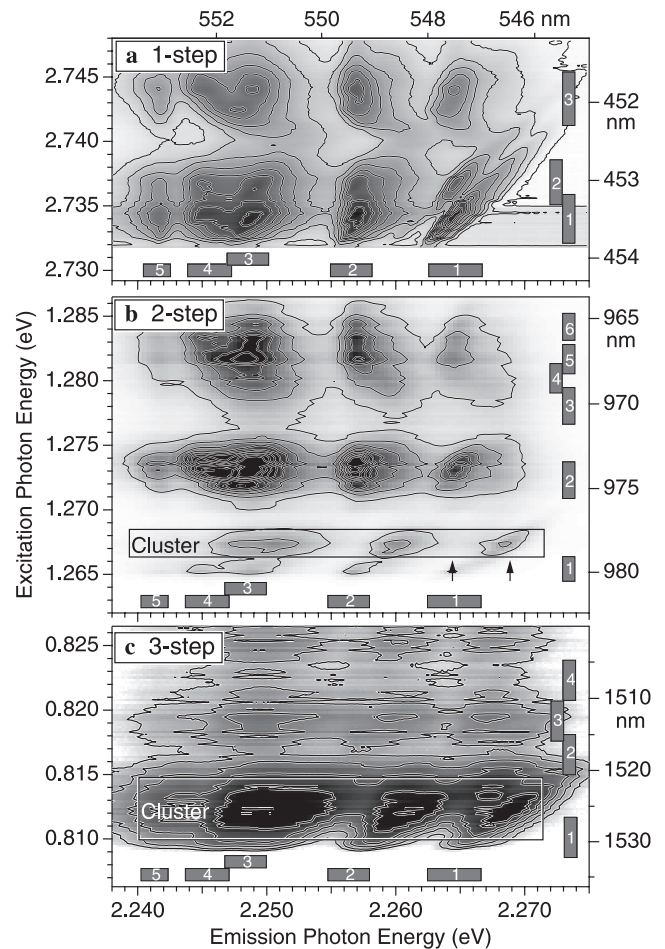[1] A complete set of data can be obtained from the authors.

Fig. 3a–c. Contour plot of CEES data of the green emission ($^4S_{3/2} \rightarrow {}^4I_{15/2}$) for **a** 1-step excitation ($^4I_{15/2} \rightarrow {}^4F_{5/2}$) at ≈ 450 nm, **b** 2-step excitation ($^4I_{15/2} \rightarrow {}^4I_{11/2} \rightarrow {}^4F_{7/2}$) at ≈ 980 nm, and **c** 3-step excitation ($^4I_{15/2} \rightarrow {}^4I_{13/2} \rightarrow {}^4I_{9/2} \rightarrow {}^2H_{11/2}$) at ≈ 1.5 µm in an Er^{3+}-doped Ti:LiNbO$_3$ waveguide. All measurements were performed for σ polarization of excitation and polarization-independent detection of the emission. The *small shaded boxes* indicate the spectral regions of excitation and emission of regular sites. Spectral ranges where cluster sites are most obvious are marked as well. For details see text

3.1 Influence of Er^{3+} diffusion doping and of Ti^{4+} ions on Er^{3+} sites

Starting out with the question of how the Er^{3+} doping method affects the Er^{3+} sites, we depict in Fig. 4b the contour plot of the CEES data taken for the green emission under direct excitation of a spot outside of the wave-guiding region [(2) in Fig. 2] which does not contain any Ti^{4+} but only Er^{3+}. The selected narrow spectral region contains just a single transition for both excitation and emission, such that each observed peak represents a different Er^{3+} environment. These different sites can be distinguished nicely and are labeled by numbers (1–11) as for the bulk material in [9]. Apart from a slight broadening of the spectral lines, the emission data of the diffusion-doped area are identical to those obtained for the congruent bulk LiNbO$_3$ doped during crystal growth (see Fig. 7 in [9]).

Expanding out of Fig. 3a the same spectral range as above for the emission light of the wave-guiding region [(1) in Fig. 2] the distinct sites are less apparent, although five sub-
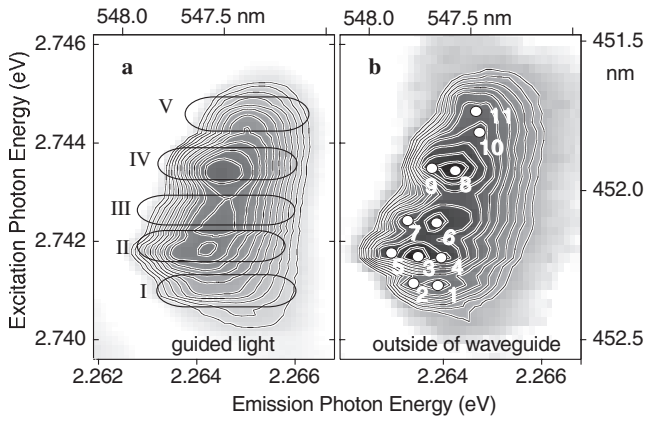
Fig. 4a,b. Expanded view for CEES data of $(^4I_{15/2} \rightarrow {}^4F_{5/2})$ direct excitation and $(^4S_{3/2} \rightarrow {}^4I_{15/2})$ emission of Er^{3+} in $LiNbO_3$ originating from **a** the light-guiding zone and **b** outside of the waveguide, i.e., (1) and (2) in Fig. 2, respectively. In the latter case, the rather weak emission was detected in back reflection to obtain maximum intensity

Fig. 5. a Relative abundance of the subgroups of Er^{3+} sites (I–V, as labeled in Fig. 4) in congruent bulk $LiNbO_3$-doped during crystal growth, as well as in diffusion-doped congruent $LiNbO_3$ outside and within the wave-guiding zone of a $Ti:LiNbO_3$ waveguide. **b** Depolarization $\frac{I_\pi}{I_\pi + I_\sigma}$ of the Er^{3+} transition chosen in Fig. 4 which is expected to be perfectly σ polarized ($I_\pi = 0$). I_π, I_σ: intensities of the π- and σ-polarized emission light

groups (I–V) can still be distinguished (see Fig. 4a). This division is well justified because we have already found in bulk material that the unresolved sites comprising these subgroups have very similar optical properties and almost identical behavior under application of external perturbations [14]. If we neglect for the moment the considerable broadening of the spectral lines, we notice that the overall appearance of the contour plots for the data taken within and outside of the waveguide are very similar, suggesting that the Er^{3+} sites are not changed drastically – at least in their nearest environment – by the presence of the Ti^{4+} ions. This finding is further supported by the almost identical relative abundances (shown in Fig. 5a) of the subgroups obtained from an evaluation of the relative integrated emission intensities for the three situations (congruent bulk, outside and within waveguide) we considered. Moreover, the polarization behavior of the subgroups is hardly changed; this can be seen in Fig. 5b, which shows the deviation from the complete σ polarization of the emission expected for perfect C_3 site symmetry in the spectral range of Fig. 4.

Even though the microscopic origin of the observed different Er^{3+} sites is still under discussion, based on results from ligand sensitive techniques [1, 15–17], it is generally accepted that at least 90% of the Er^{3+} ions are located at or in the close vicinity of a Li^+ site. The required charge compensation for the isolated Er^{3+} ions may be provided by two neighboring Li^+ vacancies or other defect arrangements resulting from the Li^+ deficiency in congruent $LiNbO_3$ [18]. The local compensation causes significant differences in the environment and, hence, is the origin of the different Er^{3+} sites, which we will refer to in the following as "regular sites". In our previous studies on bulk material [9] it could be shown that the charge compensation by single-charged defects can be classified into two groups. Firstly, we have a primary compensator located on different positions in the nearest neighborhood causing the rather significant spectral differences between the subgroups (I–V). Secondly, these groups are further subdivided due to the secondary compensator located at a larger distance. Adapting this view, we can conclude that the primary compensation is essentially identical for the different cases investigated.
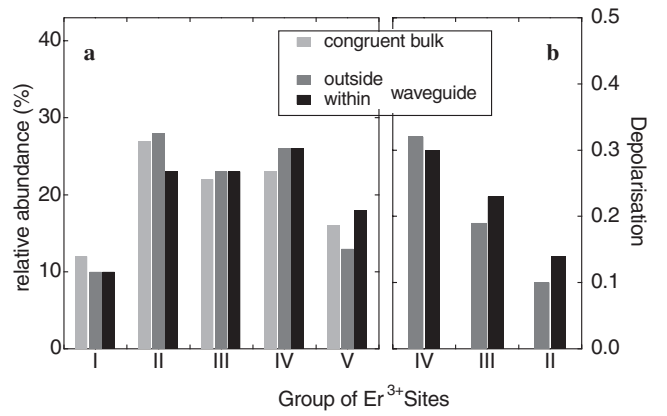
Similar to the Er^{3+} ions, the Ti^{4+} ions occupy Li^+ positions preferentially. This important information has again been obtained by studies employing various ligand-sensitive techniques [19–22]. Furthermore, transmission electron microscopy studies [20] of Ti-diffused $LiNbO_3$ indicated that structural faults are formed as a result of the excess vacancies and anti-site defects. Similarly, X-ray absorption measurements [21] indicated that above a certain Ti^{4+} concentration limit ($\approx 5 \times 10^{20}$ cm^{-3}), which is lower than the Ti content in our samples, changes in the Ti^{4+} centers appear. Both observations give evidence that a considerable degree of disorder is introduced by the Ti^{4+} doping, accounting for the inhomogeneous broadening of the spectral lines in our measurements. On the other hand, both Er^{3+} and Ti^{4+} defects are charged positively in respect to the lattice site they occupy and, for electrostatic reasons, have little tendency to attract each other. Therefore it is not surprising that in the waveguide we essentially observe only sites which are very similar to those in the Ti-free region. There is some indication for the presence of particular Ti^{4+}-related Er^{3+} sites, but the sensitivity of our method is insufficient to unambiguously distinguish them from the other more abundant sites. For 1-step excitation, only sites with an abundance of more than 5% can be detected individually. In results for emission under multistep excitation, much less abundant (cluster) sites can also be observed. They will be treated in Sect. 3.3 along with the underlying excitation processes.

3.2 Changes in optical properties and fluorescence line narrowing

In the discussion above we noticed that the optical properties of the regular Er^{3+} defects within the Ti^{4+}-doped region of the waveguide hardly change. The only apparent difference is a strong increase in the inhomogeneous width of the spectral lines. For the study of such inhomogeneously broadened transitions fluorescence line narrowing (FLN) is a well-established method. This technique is based on the fact that under narrow-line laser excitation only a certain subset of defects is excited, which should in turn show an emission

reflecting, in the ideal case, only the much smaller homogeneous linewidth. In this sense, the CEES method should also show FLN. Different from this expectation, however, in Fig. 4a as well as in the individual emission spectrum d (Fig. 6), which was extracted from it, almost no narrowing can be observed. In order to understand this apparent contradiction, one needs to remember that the narrowing only occurs if the two levels involved in excitation and emission exhibit the same sensitivity to the perturbation, causing the inhomogeneity. This is obviously not the case for the pair of transitions chosen to obtain the spectrum d in Fig. 6. However, if we select different excitation–emission transition pairs, it is possible to find combinations for which FLN actually occurs. Spectra a to c in Fig. 6 are examples in which emission transitions to the same two Stark sublevels of the $^4I_{15/2}$ ground state are shown; these transitions occur for excitation of three different sublevels of the $^4F_{9/2}$ state (see energy scheme in Fig. 6). Depending on both the excitation and the emission transition, a different degree of FLN is observed. In particular, it is interesting to see that in spectrum a the high-energy emission line is drastically reduced in linewidth, while the width of the low-energy line is hardly changed compared to spectra b and c. For a complete understanding of the variations in the FLN effect, the level dependence of the homogeneous linewidth due to the different lifetimes of the levels also has to be considered. While this effect cannot explain the differences in spectra a–c, it plays an important role in the large linewidth of spectrum d. In the contour plots of the CEES measurements, FLN becomes immediately apparent by diagonally running emission intensity distributions. An example of that can be found in the lower right corner of Fig. 3a.

Although at room temperature this level dependence of the site selectivity in excitation is less pronounced, it still
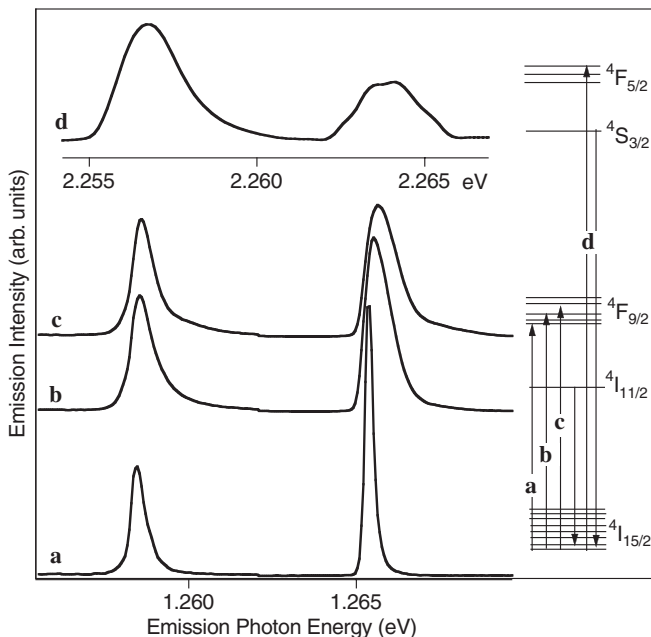
has consequences for laser applications because it makes possible the choice between cases for which either the whole inhomogeneous ensemble of ions or just selected Er^{3+} sites are excited. For instance, the lasers demonstrated at around 1.56 µm are all pumped at 1.48 µm in a transition which exhibits no site selectivity at all. On the other hand, potential 550 nm and 3 µm lasers in $LiNbO_3$ should be pumped by commercially available strong laser diodes at 980 nm, a wavelength by which a site-selective transition is excited. For that reason, in the latter case the proper choice of the wavelength is much more important. It becomes even more important if the up-conversion processes, discussed in the following, are taken into account.

3.3 Up-conversion processes

In order to study the up-conversion processes we first refer back to Fig. 3, in which the CEES data for the green emission and excitation with 980 nm and 1.5 µm corresponding to 2- and 3-step processes are depicted. Due to the larger number of levels involved, the contour plots look much more complicated, but by comparing with the direct excitation case important conclusions can be drawn. For instance, it can be seen immediately that additional sites appear (especially marked in Fig. 3) which exhibit significantly different transition energies. As in earlier studies [6, 9] we attribute them to clusters consisting of two or more Er^{3+} ions. This assignment is mainly based on their obviously much higher up-conversion efficiency. Despite their small relative number which makes them almost unobservable for direct excitation, they can easily be detected along with the regular sites for 2-step excitation and even are essentially the only center types which contribute to the green emission for 1.5 µm laser excitation. Careful comparison of the emission spectra under direct (1-step) excitation reveals that, even though the Er^{3+} concentration is higher, the number of clusters is about the same or even less in the diffusion-doped samples (both within and outside of the waveguide) compared to the samples doped in the melt. Similar to our arguments above against the existence of $Er^{3+}-Ti^{4+}$ clusters, Er^{3+} clusters are electrostatically not very favorable as long as both defects are situated on Li^+ sites. In the simple defect model, clusters or pairs in which one Er^{3+} is replacing an Nb^{5+} ion are more probable. While such configurations can be formed quite easily during crystal growth, the ionic mobility during the Er^{3+} diffusion process is much lower, making the formation of the clusters less likely.

In the following we want to discuss the up-conversion processes and the different behavior of regular and cluster sites in more detail. We will do that separately for the two excitation wavelength regions around 980 nm and 1.5 µm.

Two-step processes under 980 nm *excitation.* The observed very different up-conversion efficiency under 980 nm excitation for regular and cluster sites can only be accounted for if two different kinds of processes are considered: In the case of the spatially well-separated regular sites energy-transfer processes are negligible and up-conversion can only take place via ground state absorption (GSA) and subsequent absorption transitions out of the excited state (ESA). As only a single laser energy was used for excitation this ESA-based process,

Fig. 6. Selected spectra for (a–c) IR emission originating from subgroup II for different excitation energies and (d) green emission. For each of the four excitation energies (schematically depicted on the right) the emission transitions to the two lowest Stark sublevels of the $^4I_{15/2}$ ground state are shown corresponding to eight different excitation–emission transition pairs

indicated in Fig. 1, requires perfect energy matching of the two involved transitions. For that reason the up-converted emission cannot be observed for all Er^{3+} sites and all excitation energies for which GSA to $^4I_{11/2}$ is possible.

For the interacting ions within clusters energy-transfer processes have to be taken into account. In order to make an estimation of the up-conversion efficiency, we consider the statistically most probable cluster: a pair of Er^{3+} ions on neighboring Li^+ and Nb^{5+} sites. Within this cluster, which needs no charge compensation and for which the Er^{3+}-Er^{3+} distance is minimal, two kinds of energy-transfer processes can take place and will lead, if they occur subsequently, to an up-conversion of the excitation energy. Firstly, one ion which is excited to the $^4I_{11/2}$ state can transfer its energy to the neighboring Er^{3+} which resides in its ground state. Secondly, a cross-relaxation between two already excited ions is possible, which will lead to a relaxation of one and further excitation into a higher level ($^4F_{7/2}$) of the other. Assuming electric dipolar interaction, the Förster–Dexter type resonant energy-transfer rates of both processes can be estimated to be $\approx 10^6$ s^{-1} using the oscillator strengths determined in [3]. Even if the resonance is not perfect and phonons have to make up for the extra energy, this value is much higher than the effective relaxation rate ($\approx 10^4$ s^{-1}) for the $^4I_{11/2}$ level, leading to a favorable branching ratio. This, combined with the fact that only one resonance condition for the incident photon has to be fulfilled, explains why the up-conversion within clusters is much more efficient compared to the ESA-based process for regular sites. Besides a higher up-conversion efficiency, the difference between the two mechanisms is also reflected in the excitation spectrum. While for the ESA-type process the up-conversion efficiency spectrum is a convolution of the two absorption spectra involved, the energy-transfer-based process will spectrally only depend on the GSA. This difference can clearly be observed in Fig. 7a, in which the excitation spectra of the green luminescence under 980 nm excitation is compared for regular and for cluster sites.

Comparing again the properties in different sample types, we find that the up-conversion excitation spectra of the total green emission (Fig. 7b) in the waveguide sample are characteristically different within and outside the wave-guiding zone, despite the almost identical site distribution. Similarities in the spectra, however, occur between the stoichiometric bulk sample and the wave-guiding zone and between congruent bulk and diffusion-doped samples, respectively. This result suggests that it is not the Er^{3+} site distributions but the excitation power density that is responsible for the difference. For both the waveguide and the stoichiometric sample, the excitation density is high due to the small spatial cross-section of the guided mode in the first case and the high absorption cross-section in the latter case. The particular process causing the excitation intensity dependence is still unclear and needs further investigation. Possibilities that need to be considered are phonon-assisted up-conversion processes (as found in stoichiometric LiNbO$_3$ [9]). Depending on which type of phonon modes are excited by the intense laser and subsequent non-radiative relaxation, these processes may become either enhanced or suppressed. Effects of that kind have already been observed in several other materials by Auzel et al. [23].

Regarding practical consequences it should be noted that for waveguides at low temperature the green emission is produced at 973 nm and not at 980 nm as in bulk material (see
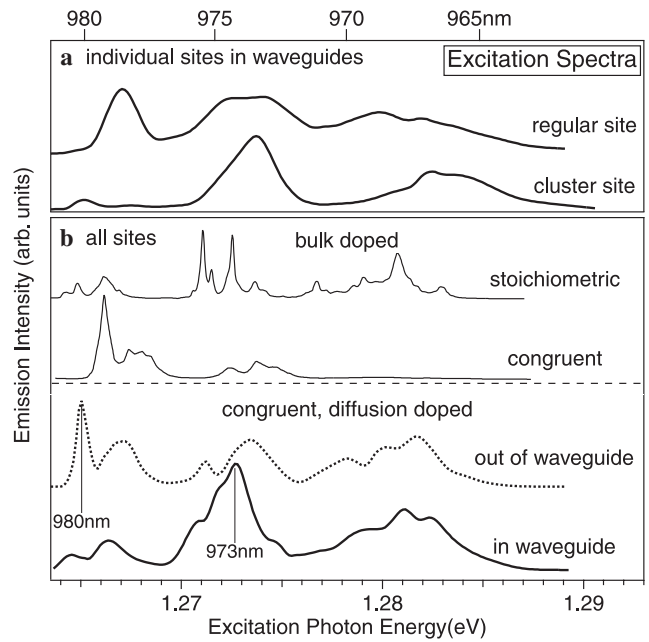

Fig. 7a,b. Excitation spectra around 980 nm of the up-converted green emission. **a** Emission intensity for a selected regular site and a cluster site obtained by taking a cross-section of the data at properly chosen emission energies, indicated by small arrows in Fig. 3b. **b** Total emission intensity for the specified types of LiNbO$_3$ samples. These spectra are obtained by summation of the emission data $I(E_{em}, E_{exc})$ over all emission energies E_{em} as a function of the excitation energy E_{exc}

Fig. 7b). Although this tendency is smeared out as the temperature is increased and phonon-assisted processes become more important, the choice of a shorter excitation wavelength may prove to be advantageous for the realization of a green up-conversion laser. By that the rather low up-conversion efficiencies found in an earlier study [3] may be improved. Attempts in this direction are currently under way.

Up-conversion processes under 1.5 μm *excitation.* Under excitation with light at around 1.5 μm, the multiplicity of possible up-conversion processes is much higher compared to 980 nm. Both 2-step and 3-step processes are present and are competing with each other.

The 3-step process for the excitation of the green emission requires perfect energy matching of three subsequent transitions ($^4I_{15/2} \rightarrow {}^4I_{13/2} \rightarrow {}^4I_{9/2} \rightarrow {}^2H_{11/2}$). Despite the (inhomogeneous) broadening of the transitions, it is extremely unlikely that for the few regular Er^{3+} sites this condition is fulfilled, and therefore we observe mostly clusters for which either a wider range of transition energies is accessible or for which at least one step of the excitation is through energy transfer. To define in more detail the type of up-conversion process at each step of excitation, we compare in Fig. 8 the GSA spectrum $^4I_{15/2} \rightarrow {}^4I_{13/2}$ with the excitation spectra of up-converted luminescence from the states $^4S_{3/2}$, $^4F_{9/2}$ and $^4I_{11/2}$. Since the non-radiative transition $^4I_{9/2} \rightarrow {}^4I_{11/2}$ is very efficient due to the small energy gap between these states, the emission from the $^4I_{11/2}$ state is a good probe to investigate the second step ($^4I_{13/2} \rightarrow {}^4I_{9/2}$) of the 1.5 μm up-conversion process. The other emission transitions require at least three steps of excitation. Using again the property that at liquid helium temperatures the excitation spectrum
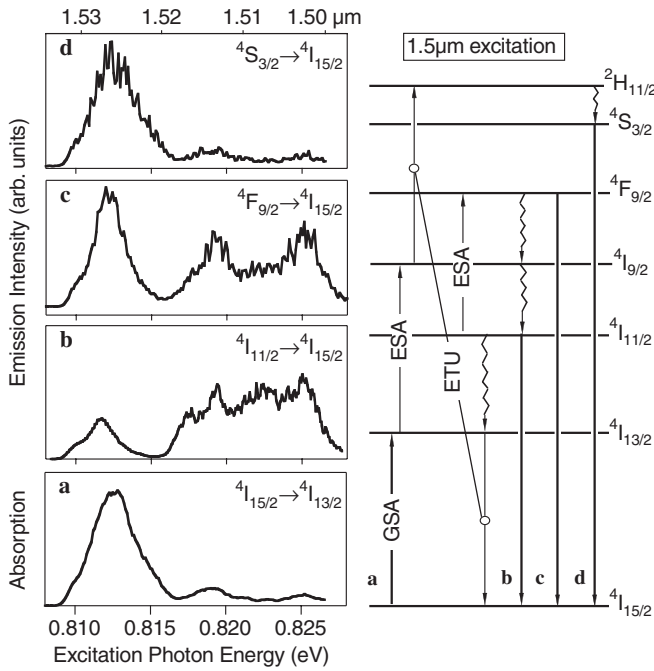
Fig. 8. a Ground state absorption ($^4I_{15/2} \rightarrow {}^4I_{13/2}$) and **b–d** excitation spectra around 1.5 µm of the total emission from the **b** $^4I_{11/2}$, **c** $^4F_{9/2}$ and **d** $^4S_{3/2}$ levels measured for the waveguide. The excitation spectra are obtained as described in Fig. 7. These transitions and the underlying excitation processes are schematically shown on the right side

emission even more complicated due to the convolution of GSA and two ESA spectra as shown in Fig. 8.

4 Summary and conclusions

We presented a comprehensive study of the optical properties and the excitation processes of Er^{3+} ions in Ti:$LiNbO_3$ waveguides and found different Er^{3+} sites which are, in their number distribution, almost independent of the doping method and the presence of Ti^{4+} ions. Despite this similarity the relative up-conversion efficiencies are drastically different for the emission probed within and outside the wave-guiding zone, showing the necessity to obtain waveguide-specific data.

The nearest neighborhood of the Er^{3+} ions remains essentially unchanged by the presence of the Ti^{4+}. Despite its high concentration the Ti^{4+} ion just induces a significant inhomogeneous broadening of the spectral lines due to variations in the long-range interaction between the two dopants.

More detailed information regarding how the diffusion profiles influence the optical properties of the Er^{3+} ions could not be obtained with the applied experimental techniques, but will be addressed by ongoing investigations using a double resonance excitation method.

In regard to planned applications of Er^{3+}:Ti:$LiNbO_3$ as 550 nm and 3 µm waveguide lasers, the observed site distribution is unfavorable. It would be desirable to enrich just those defect sites which have the best up-conversion efficiencies. Unfortunately, the higher Er^{3+} concentration in the diffusion-doped sample did not result in an enrichment of clusters. Furthermore, we have seen that in order to have the optimum up-conversion efficiency the excitation energy has to be chosen carefully. Excitation wavelengths somewhat shorter than the 980 nm used so far may prove to be more favorable both in terms of a more efficient up-conversion process and a higher number of excited ions due to a reduced selectivity.

of the up-converted luminescence reflects either the convolution of the involved GSA and ESA spectra for ESA-type processes or just the GSA spectrum for up-conversion which involves cross-relaxation (usually called energy-transfer up-conversion, ETU), we come to the following results:

1. The excitation spectrum for the emission from $^4I_{11/2}$ (Fig. 8b) is complicated and does not resemble the GSA around 1.5 µm, indicating that the second step transition is dominated by an ESA process. This also includes the possibility that the ESA occurs not at the initially excited ion but, after energy transfer, at another one for which the laser wavelength is matching better.
2. The excitation spectrum for the emission from $^4S_{3/2}$ (Fig. 8d) is very similar to that of the GSA at around 1.5 µm. From this we conclude that at least one excitation step involves energy transfer. Since we have found already that the second step is ESA type, the ETU process must occur in the third step. As shown on the right of Fig. 8, pairs of Er^{3+} ions, which have been excited into $^4I_{13/2}$ and $^4I_{9/2}$ states, can exchange their energy via cross-relaxation, which brings one Er^{3+} into $^4H_{11/2}$ and the other back to the ground state $^4I_{15/2}$.
3. The drastic difference in the excitation spectra in Fig. 8c,d for the emission from $^4F_{9/2}$ and $^4S_{3/2}$ shows that the $^4F_{9/2}$ state is not populated through relaxation from the state $^4S_{3/2}$ above, but instead through a different channel. The only possibility is a $^4F_{9/2}$ excitation involving a third step transition starting from the state $^4I_{11/2}$ which is populated via fast nonradiative relaxation from $^4I_{9/2}$. This $^4I_{11/2} \rightarrow$ $^4F_{9/2}$ transition is found to be of ESA type, which makes the observed excitation spectrum for the $^4F_{9/2} \rightarrow {}^4I_{15/2}$

References

1. I. Baumann, R. Brinkmann, M. Dinand, W. Sohler, L. Beckers, C. Buchal, M. Fleuster, H. Holzbrecher, H. Paulus, K.-H. Müller, T. Gog, G. Materlik, O. Witte, H. Stolz, W. von der Osten: Appl. Phys. A **64**, 33 (1997)
2. W. Sohler, H. Suche: In *Integrated Optical Circuits and Components: Design and Application*, ed. by E.J. Murphy, (Marcel Dekker, New York 1999) pp. 127–159
3. V. Dierolf, A.B. Kutsenko, C. Sandmann, F. Tallian, W. von der Osten: Appl. Phys. B **68**, 767 (1999)
4. M.J.F. Digonnet (Ed.): *Rare Earth Doped Fiber Lasers and Amplifiers* (Marcel Dekker, New York 1993) and references therein
5. L. Nunez, B. Herreros, R. Duchowicz, G. Lifante, J.O. Tocho, F. Cusso: J. Lumin. **60–61**, 81 (1994)
6. D.M. Gill, J.C. Wright, L. McCaughan: Appl. Phys. Lett. **64**, 2483 (1994)
7. W. Jia, K.-S. Lim, H. Liu, Y. Wang, J.J. Lu, S.I. Yun, F.E. Fernandez, W.M. Yen: J. Lumin. **66–67**, 190 (1996)
8. O. Witte, H. Stolz, W. von der Osten: J. Phys. D **29**, 561 (1996)

810

9. V. Dierolf, M. Koerdt: Phys. Rev. B **61**, 8043 (2000)
10. V. Dierolf, A.B. Kutsenko, W. von der Osten: J. Lumin **83–84**, 487 (1999)
11. B. Herreros, G. Lifante, F. Cusso, P.D. Townsend, P.J. Chandler: J. Lumin. **72–74**, 198 (1997)
12. I. Baumann, S. Bosso, R. Brinkmann, R. Corsini, M. Dinand, A. Greiner, K. Schäfer, J. Söchtig, W. Sohler, R. Wessel: IEEE J. Sel. Top. Quant. Electron. **2**, 355 (1997)
13. M. Dinand, W. Sohler: J. Quant. Electron. **30**, 1267 (1993)
14. V. Dierolf, A.B. Kutsenko, C. Sandmann, Th. Tröster, G. Corradi: J. Lumin. **87–89**, 989 (2000)
15. A. Lorenzo, H. Loro, J.E. Munos Santiuste, M.C. Terrile, G. Boulon, L.E. Bausa, G. Garcia Sole: Opt. Mater. **8**, 55 (1997)
16. L. Rebouta, M.F. da Silva, J.C. Soares, D. Ferdinando, E. Diegues, F. Agullo-Lopez, J. Tornero: Appl. Phys. Lett. **70**(9), 1070 (1997)
17. T. Gog, M. Griebenow, G. Materlik: Phys. Lett. A **181**, 417 (1993)
18. A.A. Kaplyanskii: private communication
19. C. Zaldo, C. Prierto, H. Dexpert, P. Fessler: J. Phys. Cond. Matter **3**, 4135 (1991)
20. M.E. Twig, D.M. Maher, S. Nakahare, T.T. Sheng, R.J. Holmes: Appl. Phys. Lett. **50**(9), 501 (1987)
21. P. Skeath, W.T. Elam, W.K. Burns, F.A. Stevie, T.H. Briggs: Phys. Rev. Lett. **59**(17), 1950 (1987)
22. T. Gog, M. Griebenow, T. Harasimowich, G. Materlik: Ferroelectrics **153**, 249 (1994)
23. F. Pelle, F. Auzel: J. Lumin. **87–89**, 989 (2000)